Received: 13 November 2024 | Revised: 5 March 2025 | Accepted: 11 April 2025 | Published online: 29 April 2025

RESEARCH ARTICLE

Artificial Intelligence and Applications
2026, Vol. 4(1) 111–124
DOI: 10.47852/bonviewAIA52024795

BON VIEW PUBLISHING

Design and Simulation Research of Supine Rehabilitation Robot

Yifan Zhao[1], Quanyu Wu[1,*], Jiaqi Fan[1], Shuyan Xiao[1], Yongxing Wang[1], Xiaojie Liu[1] and Lingjiao Pan[1]

[1]*School of Electrical and Information Engineering, Jiangsu University of Technology, China*

Abstract: Many existing rehabilitation robots are designed with limited functional adaptability. To better assist patients with lower limb deficiencies in rehabilitation, this paper presents a new supine rehabilitation robot designed specifically for the motor rehabilitation needs of the human lower limb. To assess the feasibility of the proposed rehabilitation robot, a coupling model of the supine rehabilitation robot and human musculoskeletal system was constructed. The gait model and the human-robot coupling model were visualized and biomechanically analyzed using OpenSim. This simulation analysis compared changes in muscle activity during gait and coupled motion. The simulation results demonstrate that coupled exercise more effectively stimulates the hip and knee joint-related muscle groups. Additionally, the training targets a broader range of muscle types, with significant improvements observed in the lumbar-iliac muscle group, broad fascia tensor, adductor muscle group, and suture muscles, showing enhancement rates of 131%, 200%, 571%, and 310%, respectively. These findings confirm that the recumbent rehabilitation robot designed in this study is capable of facilitating effective rehabilitation for the human body and lower limbs.

Keywords: supine rehabilitation robot, OpenSim simulation, musculoskeletal model, coupled motion, biomechanical analysis

1. Introduction

With the continuous progress of society, there were 143.9 million elderly adults (aged 65 years or older) living in China at the end of 2015, accounting for 10.5% of the total population [1]. Stroke is a common cerebrovascular disease with high morbidity, mortality, disability, and recurrence rates [2]. In addition, the aging of society has increased the fracture rate in the elderly, causing a significant increase in the number of patients with motor dysfunction [3]. For patients with lower limb dysfunction, lower limb exoskeleton rehabilitation robots integrate science and technology into rehabilitation devices, which helps to accelerate the recovery of their motor functions, among which exoskeleton type rehabilitation robots are more widely used [4, 5].

There have been a number of research results on lower limb rehabilitation devices, for example, end-suspended lower limb rehabilitation training equipment [6], a wearable device for lower limb rehabilitation training [7, 8], and a combination sitting-lying lower limb rehabilitation training device [9]. However, different patients have different needs for the trajectory of rehabilitation training at different stages of rehabilitation, and a single training posture leads to a restricted range of limb movement. Therefore, it is difficult for such devices to meet the needs of patients at different stages of rehabilitation [10], while the rehabilitator designed in this paper has a wider range of motion and can perform rehabilitation exercises with multiple degrees of freedom.

OpenSim is a biomechanical simulation software for modeling and analyzing the musculoskeletal system. It obtains joint angles and joint moments through inverse kinematics and inverse dynamics solvers for visualization and analysis [11]. As the research on rehabilitation robots is deepened, it becomes challenging to realize the synergistic control of rehabilitation robots and human movement. Researchers at home and abroad have used OpenSim to explore the interaction between exoskeleton robots and human musculoskeletal models under different conditions. Song et al. [12] aimed at the problem that the existing ankle rehabilitation robot is difficult to fully fit the complex motion of the human ankle joint. A new 4-DOF parallel ankle rehabilitation structure was proposed, but the interaction force of the structure with the human body was difficult to obtain. A study by Delgado et al. [13] investigated the effect of shoulder motion geometry on exoskeleton design for upper arm rehabilitation tasks. The results showed that shoulder elevation is very sensitive to the orientation of the shoulder joint axis. Gordon et al. [14] presented an effective framework that combines detailed biomechanical modeling and weighted multi-objective optimization to allow fine-tuning of robot behavior based on the specifications of the task at hand. Fan et al. [15] proposed an OpenSim-based exoskeleton design method, which embedded the mechanical structure of the exoskeleton into the musculoskeletal model of the human body to perform a coupled simulation, so as to obtain the exoskeleton-assisted specific human joints and muscles. Shi et al. [16] aimed at the problem of insufficient evaluation of rehabilitation effects during the use of lower limb exoskeleton. Human-machine coupled motion analysis was carried out using OpenSim, providing theoretical support for the optimal design of lower limb exoskeleton. Feng et al. [17] designed a flexible lower limb booster exoskeleton that uses a flexible elastic band energy storage device and uses OpenSim in order to realize its optimal

*Corresponding author: Quanyu Wu, School of Electrical and Information Engineering, Jiangsu University of Technology, China. Email: wuquanyu@jsut.edu.cn

booster scheme to achieve the effect of boosting human lower limb muscles while walking. Our team has also worked in lower extremity rehabilitation. Li et al. [18] designed a traction lower limb rehabilitator and proposed a lower limb movement intention recognition method and an active control model based on surface electromyographic signals.

This paper consists of 3 parts. Firstly, a 6-degree-of-freedom horizontal rehabilitation robot is designed to address the existing lower limb rehabilitation robot with a low degree of freedom and the difficult problem of dynamic matching between the rehabilitation device and the human joints; subsequently, a coupling model between the lower limb rehabilitation robot and the human musculoskeletal system is constructed by using the OpenSim platform, and the muscle groups of the lower limb are merged to pave the way for subsequent biomechanical analyses; and finally, the muscle activities under gait movement and robot-assisted movement were analyzed by biomechanical simulation, so as to evaluate the rehabilitation effect of the rehabilitation robot.

2. Modeling of Recumbent Rehabilitation Robot

2.1. Overall model design

The usability of traditional lower limb rehabilitation robots is poor, mainly due to their large size, heavy mass, and integrated design, which makes it difficult for patients to wear and carry them by themselves. In addition, the movement patterns of traditional lower limb rehabilitation devices are relatively limited, making it difficult to provide personalized rehabilitation training and unable to fully meet the needs of different patients. Therefore, when designing rehabilitation robots, the flexibility of handling, the convenience of quick donning and doffing, and the diversity of rehabilitation training should be considered.

The structure of the designed recumbent rehabilitation robot is shown in Figure 1, which is mainly composed of a 6-degree-of-freedom robotic arm structure and a lower limb fixation structure. The multi-degree-of-freedom design can simulate a more natural human movement trajectory, which can carry out sagittal and coronal rehabilitation movements, and only need to fix the calf and foot joints to perform rehabilitation, which makes it more convenient to put on, take off, and carry. Compared with traditional rehabilitation equipment, this design does not need to manually adjust the length of the rehabilitator and can automatically adapt to the leg length of different patients, improving ease of use. Meanwhile, the robot adopts the prone training mode, which is especially suitable for patients in the early stage of rehabilitation and reduces the risk of secondary injury. Among them, the lower limb fixation mechanism consists of a base, side plate, bending plate, support pad, wrist guard, bandage, mounting strap hook, mounting strap hook ring, foot pad, support plate, and so on.

Figure 1
Overall structure diagram of rehabilitation robot

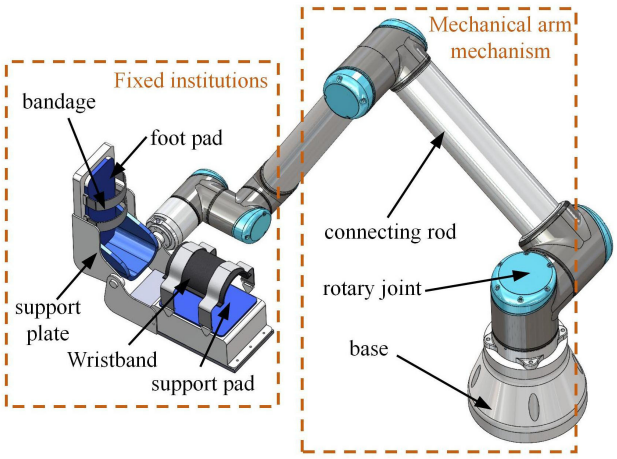

The robotic arm mechanism consists of a base, two connecting rods, and six integrated joints. The designed integrated joints are shown in Figure 2, which are mainly composed of a harmonic reducer, frameless torque motor, actuator, pin-type holding brake, and high-and low-speed encoder, and other components. The transmission path is a frameless torque motor, harmonic reducer, and output flange. In order to reduce the maintenance cost of the external alignment and to prevent the cable from breaking and causing operation inconvenience, the hollow alignment design is adopted. The wiring harness enters from the bottom of the integrated joint and is plugged into the driver, which then passes to the motor and brake, and finally to the next level of joint through the output of the hollow sleeve.

Figure 2
Schematic diagram of integrated joint structure

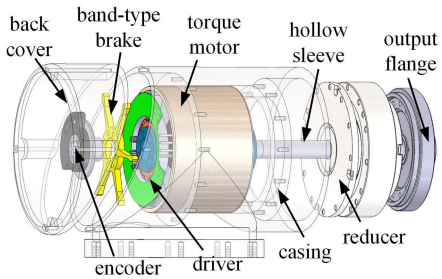

2.2. Working principle

According to the human body size of Chinese adults in Tables 1 and 2, the size of the rehabilitation robot is designed, the height of the human body is selected as 1814 mm, the length of its lower limbs is 942 mm, the arm length of the robot's arm is designed as 1200 mm, and the foot width of the mechanical leg structure is designed as 110 mm as well as the thickness of the calf, which is designed as 160 mm. when the lower limbs of the rehabilitated patients are in the workspace of the arm structure, the rehabilitation conditions can be met.

The setup of the degrees of freedom and the specific dimensions of this rehabilitation robot are shown in Figure 3. The mechanism locates the human ankle joint by means of three joints close to the base. Among them, motion axis J2 and motion axis J3 are parallel to each other, and these two joints can determine the position of the ankle joint axis in the sagittal plane. The axis of motion J1 is oriented at a right angle to J2 and J3, enabling the positioning of the ankle joint axis at any point within the coronal plane. Variations in the placement of the human ankle joint axis within the sagittal plane lead to differing angles at the hip and knee joints. The motion axis J6 is designed to synchronize with the ankle joint axis, facilitating the adjustment of the patient's lower leg position. This mechanism prevents potential injuries to the patient's lower limb that might occur if the limb reaches a dead

Table 1
Adult male body measurements

Age gender	Adult male (18–60 years old)						
Percentile	1	5	10	50	90	95	99
Height/mm	1543	1583	1604	1678	1754	1775	1814
Thigh/mm	413	428	436	465	496	505	523
Calve/mm	324	338	344	369	396	403	419
Thickness/mm	103	112	116	130	146	151	160
Foot length	223	230	234	247	260	264	272
Foot width	86	88	90	96	102	103	107

Table 2
Adult female body measurements

Age gender	Adult female (18–60 years old)						
Percentile	1	5	10	50	90	95	99
Height/mm	1449	1484	1503	1570	1640	1659	1697
Thigh/mm	387	402	410	438	467	476	494
Calve/mm	300	313	319	344	370	376	390
Thickness/mm	107	113	117	130	146	151	160
Foot length	208	213	217	229	241	224	251
Foot width	78	81	83	88	93	95	98

Figure 3
Schematic diagram of rehabilitation robot degrees of freedom

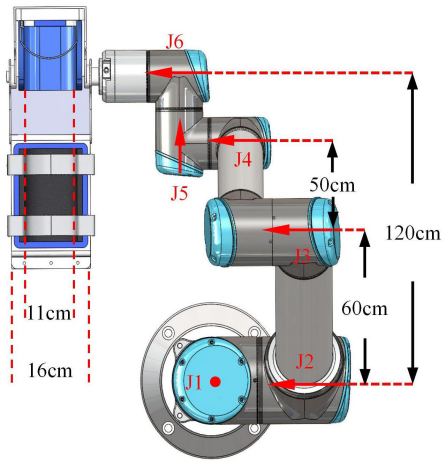

spot during rehabilitation. When rehabilitating different patients, the robotic arm module can change different positions to control the patient through the end. The working space of the end of the arm is larger than the working space of the patient's lower limbs, which enables the patient to perform rehabilitation exercises. The remaining two rotational degrees of freedom are used to realize the rehabilitation switch of both feet.

3. Modeling Human Musculoskeletal

3.1. OpenSim modeling theory

OpenSim is an open-source application of biomechanical analysis and research tool platform developed by Stanford

Figure 4
Hill muscle-tendon mechanics model

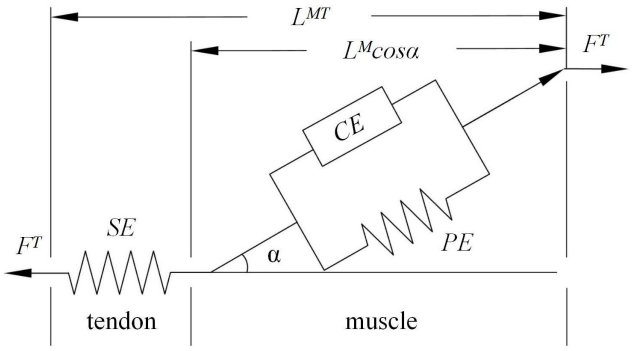

University, which has the advantages of fine control of muscle morphology parameters, small computational errors, and fast computation speed [19]. The OpenSim software modeling theory is derived from Hill's equation as well as Hill's three-element model of muscle [20–22].

The tendon complex comprises three muscle models: the contractile element (CE), the parallel elastic element (PE), and the series elastic element (SE), as illustrated in Figure 4. Among them, CE is mainly composed of myoplasmic globulin and actin fibers, which can generate active tension; PE is composed of myoplasmic globulin, actin fibers, and transverse bridges, which behave as a fully elastic body; SE is mainly composed of myofibrillar membranes, muscle bundle membranes, etc., which behave as a nonlinear elastomechanical property; and FT, α, LM, LMT, respectively, are the tendon tension, the myofibrillar pinnation angle, the myofibrillar length, and the muscle-tendon length. A complex musculoskeletal model needs to be driven by 50 or more muscle-tendon units.

Thelen [23] divided the framework into specific active and specific passive fitnesses, where the total fitness consists of the active and passive portions scaled by activation, and the active portion f_1 is represented as follows:

$$f_1 = \frac{F^M}{F_O^M} \tag{1}$$

In Formula (1), F^M is the muscle force; F_O^M is the maximum isometric force.

Specific passive muscle force $f2$ is represented by the exponential function:

$$f_2 = \frac{\exp\{[k^a(L^M - 1)/l^M]\} - 1}{\exp(k^a) - 1} \tag{2}$$

In Formula (2), k^a is an exponential parameter; l^M is passive muscle change.

In kinetic simulation, the muscle is also affected by both activation and contraction dynamics. Ideally, the muscle excitation signal e and activation s can be expressed by the first-order nonlinear differential equation:

$$\frac{ds}{dt} = \frac{e - s}{\tau_s(s,e)} \quad \tau_s(s,e) = \begin{cases} \tau_{in}(0.5 + 1.5s) & e > s \\ \tau_{de}/(0.5 + 1.5s) & e < s \end{cases} \tag{3}$$

In Formula (3), τ_{in} is the activation increase time constant; τ_{de} is the activation decay time constant. The increase or decrease in activation

is related to the amount of calcium ions as well as the release and diffusion of calcium ions.

The muscle-tendon contraction dynamics characterization interprets the interaction between the special properties of muscle as a coupling of activation, force, length, and velocity and the elastic tendon, where the contraction velocity of the muscle fibers V^M is assumed to be a function of:

$$V^M = (0.25 + 0.75s)V_{\max}^M \frac{\tilde{F}^M - sf_1}{b} \quad (4)$$

In Formula (4), $V_{\max}^M$ is the maximum contraction velocity of muscle fibers; b depends on whether the muscle fiber is Increasing or decreasing.

3.2. Modeling lower extremity musculoskeletal

OpenSim's musculoskeletal model is a complex dynamical system combining rigid bodies, joints, and muscles, which is stored as a text file and consists of a body, joints, forces, constraints, and controllers. The body is the key skeleton with a geometrical form and inertial properties; the joints and their constraints connect the relative actions between the bones, and the forces cover the internal forces from the muscles and ligaments as well as the external forces interacting with the ground. In addition, the model contains several marker points to locate the positions where the limb motion information is captured.

The officially provided musculoskeletal gait model for the lower limbs, Gait2392-simbody, was used, which has 23 joint degrees of freedom and 92 muscles, as shown in Figure 5. Based on the selected gait model to build the musculoskeletal recumbent model, when building the recumbent model, the upper body and the ground will produce contact force. The foot-ground contact force model, Hunt-Crossley, is often used to predict the change in the ground reaction force in the study of the gait movement of the gait model [24, 25]. Although the prone setup features extensive contact between the back and surface, accurately defining contact force parameters remains challenging, and research primarily focuses on lower limb movement in this posture. To stabilize the model's back, we implemented a weld constraint linking the upper torso to the surface.

3.2.1. Body module design

To analyze the human-robot coupling system, a coupling model of the human body and the rehabilitator was developed using OpenSim software. First, the lower limb rehabilitation robot model built by SolidWorks software was disassembled into modules of rotary axes and connecting rods, and exported to the STL (stereolithography) file format. Then, XML (extensible markup language) files of mass, center of mass position, and rotational inertia were determined for each module. Finally, the STL files were copied to the Geometry folder in the installation directory of OpenSim software, and the output position information was written into the XML file of the human model in Notepad. The human-machine coupling model was constructed through the constructor module, the key module, and the constraint module. The specific coupling process is shown in Figure 6.

The model is created by using the BodySet command and contains the definition of the module's name, mass, center of mass position, and inertia parameters, as well as the STL file output through the attached_geometry association for the model's display, and the module's scaling factor, transparency, and color in the XYZ axis. A total of five body modules are defined,

Figure 6
Human-machine coupling flowchart

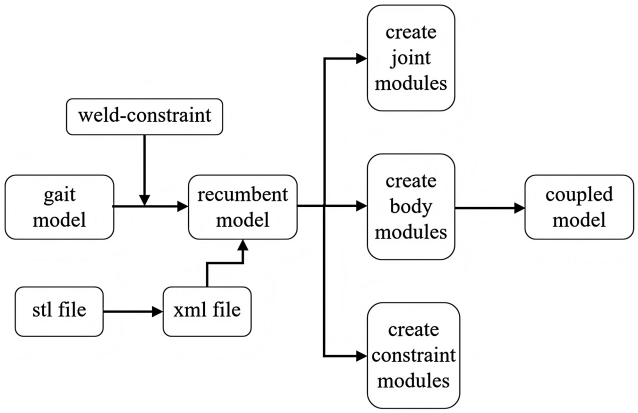

Figure 5
Lower limb musculoskeletal gait model and lower limb musculoskeletal recumbent model

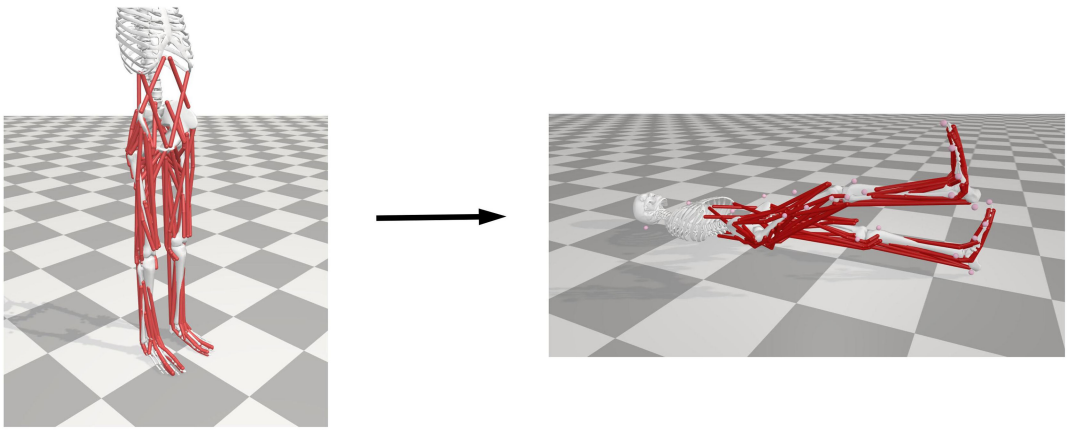

including base joint complex, joint linkage complex 1, joint linkage complex 2, end joint complex, and lower limb fixation body module.

3.2.2. Joint module design

The CustomJoint command under the JointSet command is used to define inter-module kinematic coordinates and kinematic transformations, including the definition of the PhysicalOffset Frame command, the definition of the translational and rotational offsets for the initial positions of the joint parent and joint children, and the definition of the coordinates command, including the definition of the initial rotational angle and the range of rotational angles. The definition of the coordinate command, which includes the definition of the initial rotation angle and the range of rotation angle, describes the generalized coordinates used to describe the range of motion of each rotation axis of the rehabilitation robot. The definition of the SpatialTransform command, which includes the definition of the rotational translational motion in the XYZ axes, is used to describe the mode of motion of the generalized coordinates. A total of four generalized coordinates are defined, including the rotation axis of the hip joint adduction and abduction, the rotation axis of the hip joint anteflexion and retroflexion, the rotation axis of the knee joint retroflexion, and the ankle positional adjustment axis.

3.2.3. Constraint module design

Finally, two constant distance constraints were created using the ConstraintSet command as Rfoot1 and Rfoot2, including the definition of the constraint body, constraint points, and constraint distances, in which the Achilles tendon calcn_r and lower limb fixation body module of the right foot were involved in the Rfoot1 constraint, and the tibia_r and the lower limb fixation body module of the right side were involved in the Rfoot2 constraint The two constraints sets are used to dress and immobilize the lower limb on the rehabilitation robot. The coupling model between the lower limb rehabilitation robot and the human musculoskeletal model is constructed by the above-embedded code modular design method, as shown in Figure 7.

3.2.4. Muscle distribution design

In order to facilitate the muscle analysis, this paper refers to the method of Pan et al. [26]. Muscles with similar functions and close anatomical locations were combined and analyzed, as shown in Figure 8, which included GL (gluteus group: gluteus maximus, gluteus medius, gluteus minimus, and pyriformis), PSOAS (lumbar iliacus group: iliacus and psoas major), SE (popliteus group: semimembranosus and semitendinosus muscle), BF

Figure 8
Distribution of lower limb muscles

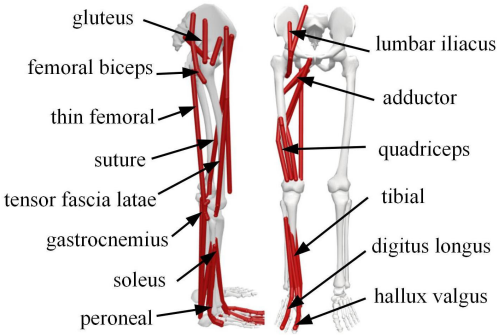

(femoral biceps group: long head of biceps femoris and short head of biceps femoris), ADD (adductor group: adductor longus, adductor brevis, and adductor magnus), GAS (gastrocnemius group: medial head of gastrocnemius and lateral head of gastrocnemius), VAS (quadriceps group: medial femoris, intermediary femoris, and lateral femoris), DIG (digitus longus group: flexor digitorum longus and extensor digitorum longus), HAL (hallux valgus group: flexor hallux valgus and extensor hallux valgus), PER (peroneal group: short fibula, long fibula, and third fibula), TIB (tibial group: tibialis posterior and tibialis anterior), SA (suture), GRAC (gracilis), PECT (pubococcygeus), RF (rectus femoris), TFL (tensor fascia latae), and SOL (soleus).

4. Simulation Analysis

4.1. Experimental procedure

The Opensim experimental analysis was divided into four steps, namely Scaling (labeling and scaling the model), IK (inverse kinematics), RRA (residual reduction algorithm), and CMC (computed muscle control), and the detailed flow is shown in Figure 9.

The gait model and the coupling model are marked and scaled using the Scaling Tool of the OpenSim platform. The adjusted model is input into the Inverse Kinematics Tool (IK Tool) to complete the inverse kinematics solving. Then, the inverse kinematics results are imported into the Residual Reduction Tool (RRA Tool) as the input data, and the residual reduction algorithm is used to optimize the inverse kinematics results. The modified motion files are analyzed by the Muscle Analysis Tool to obtain the muscle-tendon change

Figure 7
Human-machine coupling model

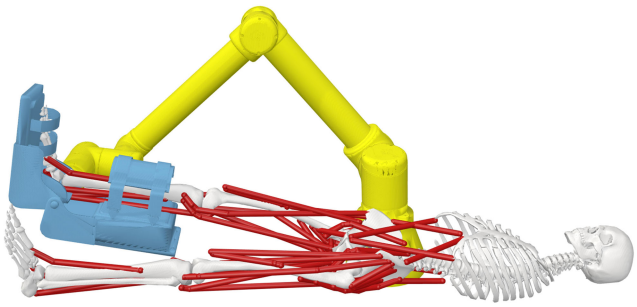

Figure 9
Experimental flow chart

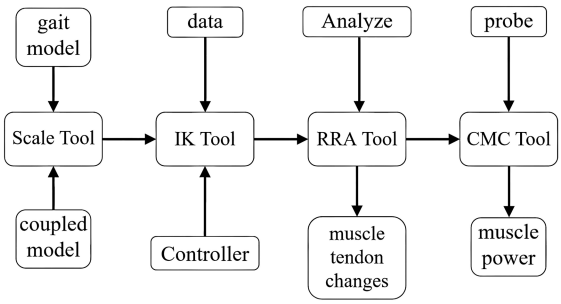

curves and muscle activity. Then, the inverse kinematics results are imported into the RRA Tool as input data to optimize the inverse kinematics results using the residual reduction algorithm. The corrected kinematics files are analyzed by the Muscle Analysis Tool, which results in the muscle-tendon change curves of the gait model and the coupling model, as well as the muscle activity, which serves as a preliminary validation of the rehabilitation effect of the rehabilitation robot. Finally, the optimized results were input into the muscle control calculation tool CMC Tool for calculation, after which the muscle force and energy metabolism of each muscle over the set time were obtained, and the rehabilitation effect of the rehabilitation robot was further evaluated according to the muscle force and energy metabolism.

4.1.1. Marking and scaling of human musculoskeletal models

In order to achieve highly accurate simulations of human movement, musculoskeletal models need to be labeled and scaled. Scaling Tool utilizes anthropometric principles to fit the model as closely as possible to the specific individual and adjusts the generic model by comparing experimental data with virtual marker points. In addition to scaling the model, the Scaling Tool can be used to optimize the position of the virtual marker points to more accurately match the experimental data, thereby adapting the musculoskeletal model to different populations and minimizing the error with the experimental data. This process can be achieved by the least squares method:

$$f_0(x) = \|Ax - b\|^2 = \sum_{i=1}^{k} (a_i^T x - b)^2 \tag{5}$$

In Formula (5), A is a $k * n$ matrix, a_i^T is a row in A, and x, b are vectors.

There are two ways to scale the model: the first is to directly input the file in the Scaling Tool window, and the second is to import the Setup_Scale.xml file through the Scaling Tool to complete the model scaling. In this paper, we choose the first method, referring to the existing data of Gait2392_Simbody model, and manually adjusting the virtual marker points to achieve data matching. The relationship between the input and output of the model file is shown in Figure 10.

The Body_Setup_Scale.xml file mentioned in the figure is the configuration file of the scaling tool, which is used to set parameters such as the model file and the weights of the markers, and its content includes the following parts: ScaleTasks – used to specify the weights of the markers, and the value of the weight is relative; the higher the weight, the smaller the error between the position of the virtual markers and the experimental markers. The higher the weight, the smaller the positional error between virtual markers and experimental markers, which can be used to evaluate the effect of virtual markers tracking the experimental markers. ScaleMeasurementSet adjusts the scaling of the musculoskeletal model by the pairwise distances between the experimental marker points. ScaleScaleSet allows manual adjustment of the generalized musculoskeletal model with separate scale factors in the x, y, and z directions. The Body_ScaleMarkerSet.xml file defines a set of virtual marker point data, including information on the location of marker points related to the lower limb in the musculoskeletal model and the scaling factor settings. Body_Static.trc is the marker trajectory file for the static experiments, and Gait2392_Simbody.osim is the musculoskeletal file for the gait model. Body_Scale.osim is obtained by scaling, which is the basis for coupled model scaling and is necessary for subsequent motion simulation.

Figure 10
Scale tool file input-output relationships

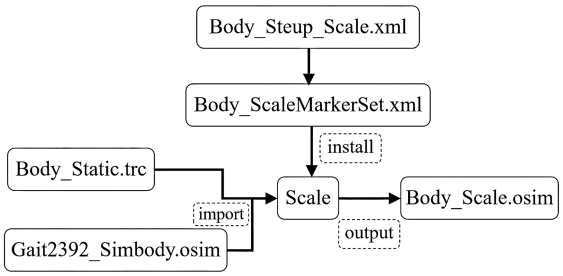

4.1.2. IK algorithm-based joint angle data solving

In the OpenSim platform, the inverse kinematics of the human lower limbs is realized by the IK Tool (Inverse Kinematics Tool). This tool loads the experimentally collected kinematic marker data into the scaled model and derives the generalized coordinates (joint angles) of the human body in the experiment through OpenSim simulation. During the procedure, the weighted least squares approach is employed to minimize discrepancies between markers and generalized coordinates, ensuring that the joint angles in the musculoskeletal model align more closely with the actual angles of the participants. Marker error refers to the difference between virtual markers and experimental markers, whereas generalized coordinate error represents the deviation between the experimental subject's generalized coordinate values and the model's computed values. By applying weighted minimization to the sum of squared errors for both marker and generalized coordinate deviations, the model's precision is ultimately enhanced:

$$S_{\min} = \sum_{i=1}^{markers} w_i \left(x_i^{\exp} - x_i^{model}\right)^2 + \sum_{j=1}^{jointangles} w_j \left(q_j^{\exp} - q_j^{model}\right)^2 \tag{6}$$

In Formula (6),

w_i: tag weight;

$x_i^{\exp}$: experiment with the position of human marker i;

x_i^{model}: model human body marking the position of i;

w_j: generalized coordinate weights;

$q_j^{\exp}$: experiment with generalized coordinate positions of the human body j;

q_j^{model}: generalized coordinate position of the model human body j.

Through the input files provided by the IK Tool, the kinematic data of the experiment can be processed to generate the optimized joint angle data files, and the relationship between its input and output is shown in Figure 11. Body_Scale.osim is the musculoskeletal model obtained by scaling in the previous section; Body_walk1.trc is the experimental marker trajectory obtained through the motion capture system; Body_coords.mot is the experimental generalized coordinate data (angle) obtained through the motion capture system; Body01_Setup_IK.xml file contains all the IK Tool setup information, including setting the weight of each marker point, which is used for evaluating the tracking effect of the virtual markers on the experimental markers. Body01_walk1_ik.mot is the kinematic result file output by IK calculation.

Figure 11
IK tool file input-output relationships

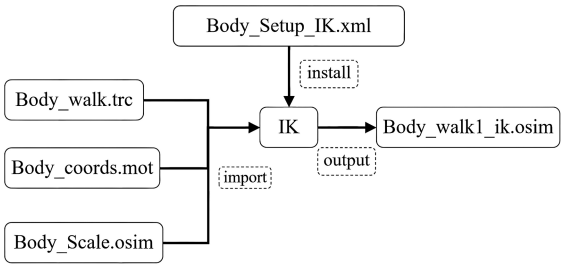

4.1.3. Optimization of joint angle data based on RRA algorithm

Coupled human-machine dynamics examines movement and computes the forces and torques responsible for generating it. Within OpenSim, inverse dynamics identifies the forces and torques driving a specific movement by solving the system's motion equations. This process constructs motion equations using kinematic parameters and mass characteristics while incorporating joint angles from inverse kinematics and ground reaction force data collected in experiments to determine the net reaction forces and torques at each joint necessary for gait execution. When solving inverse kinematics, integrating kinematic data with ground reaction forces may introduce overconstraints, creating more equations than joint variables. Additionally, deriving ground reaction forces and acceleration from labeled point kinematics may conflict with Newton's second law. To solve this problem, there are usually three methods available:

1) Change $F_{\exp}$

$$F_{\exp} + F_{residual} = ma_i \tag{7}$$

In Formula (7), this residual force may be large and the balance of motion cannot be solved by adjusting the external force alone, so this method is not feasible.

2) Change a_i

$$F_{\exp} = ma_i \tag{8}$$

In Formula (8), known as the Residual Elimination Algorithm (REA), reduces the residual force by adjusting the experimental kinematics so that it is in dynamic equilibrium with the measured ground reaction force. However, the method has some shortcomings. First, it is not realistic to completely eliminate the residual force by reducing the head, femur, and tibia to a single rigid body during modeling. Secondly, it is difficult to maintain the equilibrium state during prolonged motion without applying a small amount of force and moment during the simulation.

3) Change $F_{\exp}$ and a_i, residual reduction method (RRA)

$$F_{\exp} + F_{residual} = \sum_{i=1}^{segments} m_i(a_i - g) \tag{9}$$

In Formula (9),
$F_{\exp}$: experimental external forces;
$F_{residual}$: residual force;
m_i: body segment i quality;
a_i: acceleration of body segment i;
g: gravitational acceleration.

RRA is a forward dynamics approach that follows inverse kinematically determined model kinematics by tracking controllers to minimize the effects of modeling and labeling data processing errors. It reduces residuals by adjusting the model's center of mass and dynamically matching ground reaction forces to enable coordinated simulation of model motion over long periods of time. Muscle control computation is used as a controller that can be added to exoskeleton robot joint positions to determine mass distributions and joint kinematics that are more consistent with ground reaction forces. RRA utilizes the OpenSim platform's muscle control calculation tool (RRA Tool) and imports the Setup_RRA.xml file to complete the dynamics analysis. setup_RRA.xml file performs the dynamics calculations by referencing data from the model file, the controller, the ground reaction force, etc. The core task of Setup_RRA.xml file is to optimize the control of the objective function, j:

$$j = \sum_{i=1}^{n_x} x_i^2 + \sum_{j=1}^{n_q} w_j \left(q_j^* - q_j\right)^2 \tag{10}$$

In Formula (10),
x_i: actuator control;
w_j: weighting factor;
q_j^*: target acceleration;
q_j: model acceleration;

In the Body_RRA_Tasks.xml file, the parameters <kp>, <kv>, and <ka> are set for the proportional differential (PD) control to compute the acceleration needed to track the experimental kinematics from the IK solution. The Body_RRA_Actuators.xml file, on the other hand, defines the actuators of the model through <ForceSet>. In this study, 12 actuators are set up in the sagittal plane, in which 6 degrees of freedom between the lumbar gauntlet and the ground are driven by 6 actuators as residual actuators. The 3 translational degrees of freedom between the lumbar gauntlet and the ground are denoted by FX, FY, and FZ, respectively, while the residual moments of the 3 rotational degrees of freedom are denoted by MX, MY, and MZ. The RRA is run after the relevant parameters of the Body_Setup_RRA.xml file are set up. The input-output relationship of the RRATool file is shown in Figure 12:

4.1.4. Muscle control calculation based on CMC algorithm

After model scaling, inverse kinematics, and residual reduction, muscle control calculations are required in order to analyze muscle

Figure 12
RRA tool file input-output relationships

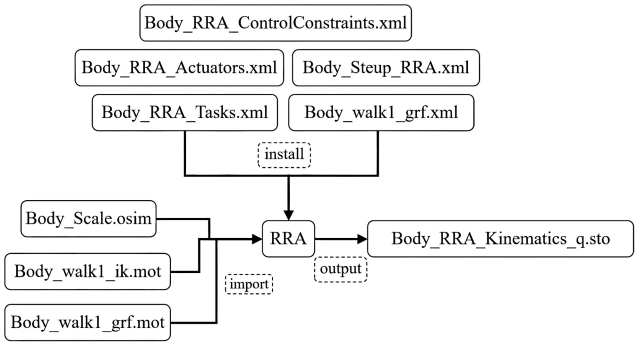

force changes and energy expenditure during movement. The muscle control is implemented by the CMCTool tool on the OpenSim platform, which uses proportional differential control and static optimization to ensure that the dynamically coupled model can track the target kinematics, minimize the errors caused by the modeling and labeling data processing, and reduce the residuals. The CMC algorithm is divided into the following three steps:

1) Calculate the desired acceleration in generalized coordinates a, which is used to drive the model coordinates b close to the experimental coordinates c, and derive the required acceleration according to the PD control law.

$$\vec{q}^{*}(t+T) = \vec{q}^{*}\exp(t+T) + \vec{k}_v\left[\vec{q}_{\exp}(t) - \vec{q}(t)\right] + \vec{k}_p\left[q_{\exp}(t) - q(t)\right] \tag{11}$$

In Formula (11),

$\vec{q}^{*}$: desired generalized coordinate acceleration;

$\vec{q}^{*}_{\exp}$: laboratory-measured generalized acceleration;

$\vec{q}_{\exp}$: laboratory-measured generalized coordinate velocities;

$\vec{q}$: generalized coordinate velocity;

$q_{\exp}$: coordinate vectors obtained by the laboratory;

$\vec{k}_v$: velocity feedback gain;

$\vec{k}_p$: position feedback gain.

2) Solve for the controller output d to generate the desired acceleration e. CMC can utilize multiple actuator types, such as joint moments. To distribute the load among multiple actuators, static optimization is applied, which can be done in two ways.

If the target speed is slow, the weighted sum of the actuator control squares plus the required acceleration error:

$$J = \sum_{i=1}^{n_x} x_i^2 + \sum_{j=1}^{n_q} w_j\left(q_j^{*} - q_j\right)^2 \tag{12}$$

In Formula (12), $\sum_{i=1}^{n_x} x_i^2$ for minimizing and distributing the load on the drive; $\sum_{j=1}^{n_q} w_j\left(q_j^{*} - q_j\right)^2$ is to make the type acceleration drive toward the desired acceleration.

For fast targets, the sum of the actuator control squares, expanded by a set of equations, achieves the desired acceleration within the optimizer's tolerances:

$$J = \sum_{i=1}^{n_x} x_i^2 \tag{13}$$

$$C_j = q_j^{*} - q_j \tag{14}$$

Often, fast targets enable efficient and accurate tracking. However, when the constraints cannot be satisfied, it may lead to failure. To avoid the failure of fast target tracking, a backup actuator can be introduced into the model to compensate for the lack of power of the original actuator.

3) Based on the computed controller, perform a forward dynamic simulation to advance the time by f. Repeat the computed acceleration, static optimization, and forward dynamic simulation until the time advances to the desired motion interval. The relationship between the inputs and outputs of the CMCTool is shown in Figure 13.

Figure 13
CMC tool file input-output relationships

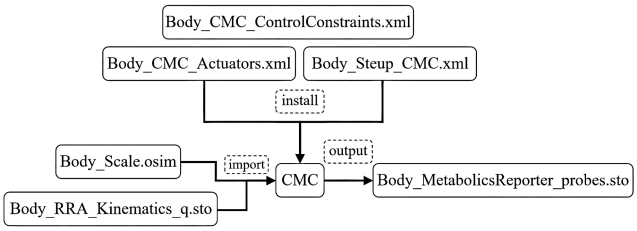

Body_Setup_CMC.xml is a configuration file for the CMCTool that defines the behavior of the tracking controller and the control parameters of the actuators. Body_RRA_Kinematics_q.sto is the kinematics data file obtained from RRA. The Body_CMC_ControlConstraints.xml file defines the constraints of the model's actuators, including alternate and residual actuators, and specifies the excitation ranges (maximum and minimum) for each actuator. Body_CMC_Actuators.xml contains specific information about the residual and alternate actuators. During the CMC run, the metabolic probes perform calculations in the background, and at the end of the CMC run, a MetabolicsReporter_probes.sto file is generated, which records the energy changes for each muscle and the total energy expenditure for all muscles.

4.2. Lower extremity gait simulation

By importing the existing high-precision motion trajectory files for the constructed musculoskeletal gait model, guiding the model movement, using the IK tool to perform the inverse kinematic simulation, adjusting the mass distribution of each skeletal structure of the torso through the residual reduction tool, correcting the inverse kinematic curves of the IK inverse solution, and finally observing the degree of muscle activity in the walking state. The changes in the angles of the joints of the lower limbs during a gait cycle obtained by simulation are shown in Figure 14, with the hip joint angle changing from −18° to 27°; the knee joint angle changing from −60° to 0°; and the ankle joint angle changing from −15° to 10°.

Figure 14
Changes in joint angles of lower limbs

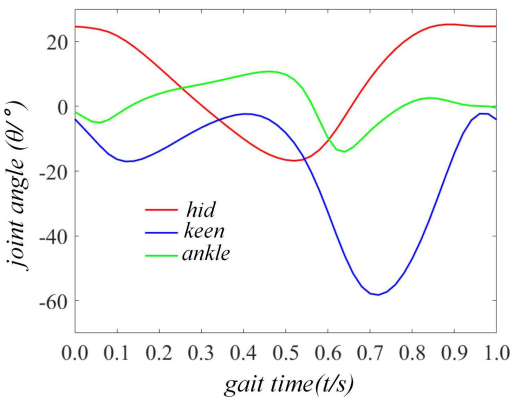

Figure 15
Human lower limb gait walking cycle

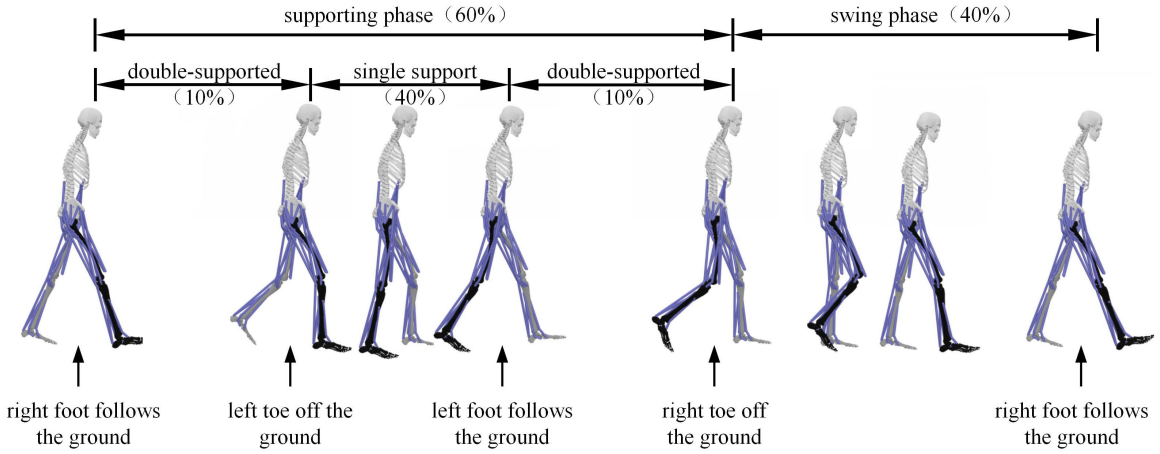

The lower limb gait during human walking shows a periodicity [27], the structure of which is shown in Figure 15 [28]. A complete gait cycle consists of a support period, which accounts for 60% of the entire gait cycle, and a swing period, which accounts for 40%. Among them, the support phase is composed of three phases and is decomposed by taking the human right leg as an example: the initial double-support phase makes up 10%, beginning when the right foot touches the ground and ending as the left toe lifts off. The single-support phase constitutes 40%, starting as the left toe lifts off the ground and ending when the left foot touches down. The second double-support phase also comprises 10%, starting when the left foot touches the ground and ending as the right toe lifts off.

4.3. Action design for coupled models

In the sagittal and coronal planes of the human body, the lower limbs possess five movement freedoms, comprising two at the hip (abduction and adduction, forward, and backward flexion-extension), one at the knee (bending), and two at the ankle (dorsiflexion and plantarflexion, along with eversion and inversion) [29]. The motion ranges for these five freedoms are detailed in Table 3 [30].

By applying auxiliary moments to the rotary joints J1, J2, J3, and J6 in the XML file of the rehabilitator, the human body is assisted in completing the rehabilitation movements. Two kinds of rehabilitation movements were designed. The first set of movements, by adding auxiliary moments to the rotary joints J2 and J3, drove the lower limb to perform the combined movements of hip joint forward flexion and knee joint backward extension, with the maximum forward flexion angle of 100°, the maximum backward extension angle of 135°, and the movement time of 9s, as shown in Figure 16. In the second set of movements, by adding auxiliary torque to the rotary joint J1, the lower limb was driven to perform hip joint adduction and abduction movements with a maximum adduction angle of 20°, a maximum abduction angle of 45°, and a movement time of 13s, as shown in Figure 16.

Table 3
Range of motion of each joint of the lower limb in normal adults

Joint	Forward	Range	Reverse	Range
Hip	inward	0~30°	outward	0~45°
	forward bend	0~130°	backward stretch	0~50°
Knee	forward bend	0°	backward stretch	0~135°
Ankle	plantarflexion	0~55°	dorsiflexion	0~25°
	inversion	0~50°	eversion	0~45°

4.4. Muscle analysis

During human movement, each action involves the concerted work of multiple muscle groups, and the involvement of different muscle groups varies. The angle of joint movement and the force in muscle activity are closely related to changes in muscle length, which reflects the activity and motivational state of the muscle. The goal of rehabilitation training is to enhance the proprioception around the joints and to correct the lack of muscle strength. By simulating different movement states, the muscle-tendon length changes of the lower limb muscle groups were observed to analyze the activity level of the muscle groups. The rehabilitation effect of the recumbent rehabilitation robot was evaluated by comparing the muscle activity under rehabilitation training and gait exercise.

To verify the feasibility of the recumbent rehabilitation robot in assisting patients in rehabilitation training, muscle analysis was performed and compared between gait exercise and designed rehabilitation maneuvers. By using the Analyze tool to muscle analyze the corrected gait motion data files and movement data files, the trends of muscle-tendon changes under the gait cycle of the right foot and the trends of muscle-tendon lengths under the two movements were obtained, as shown in Figure 17, where the vertical coordinate is the muscle length in m and the horizontal coordinate is the time in s. Among them, Figure (a) and (b) show the muscle changes of the hip-knee muscle group under the gait movement, Figure (c) and (d) show the muscle changes of the hip-knee muscle group under Action 1, and Figure (e) shows the muscle changes of the hip joint muscle group under Action 2.

In performing the muscle analysis, the distribution of the hip and knee muscle groups is discussed. The hip-related muscle groups included GL, ADD, PSOAS, BF, SE, PECT, GRAC, RF, SA, and TFL, and the knee-related muscle groups included BF, SE, GAS, VAS, RF, SAR, and GRAC, of which BF, SE, GRAC, RF, and SA were the common muscle groups of the hip and knee joints, which acted on both joints simultaneously. Among them, the SE muscle group only considers the muscle changes of the long head of the biceps femoris when analyzing only the hip joint

Figure 16
Hip flexion and knee extension movements and hip joint adduction and abduction movements

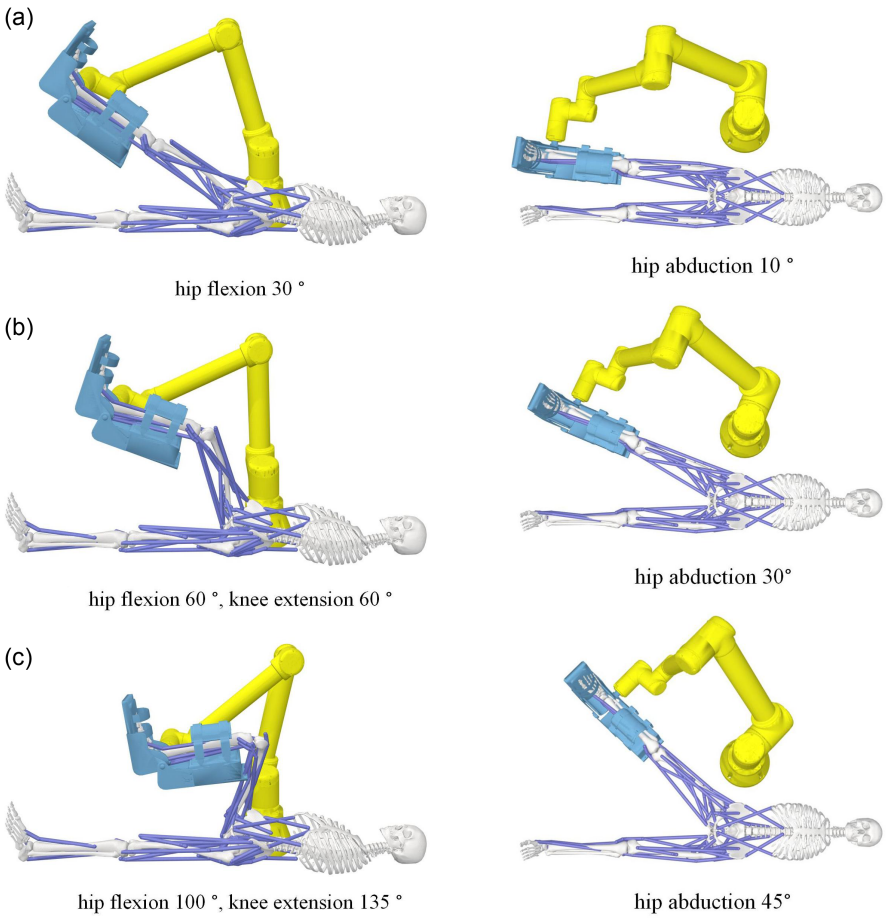

Figure 17
Muscle tendon length changes of hip and knee joint-related muscle groups

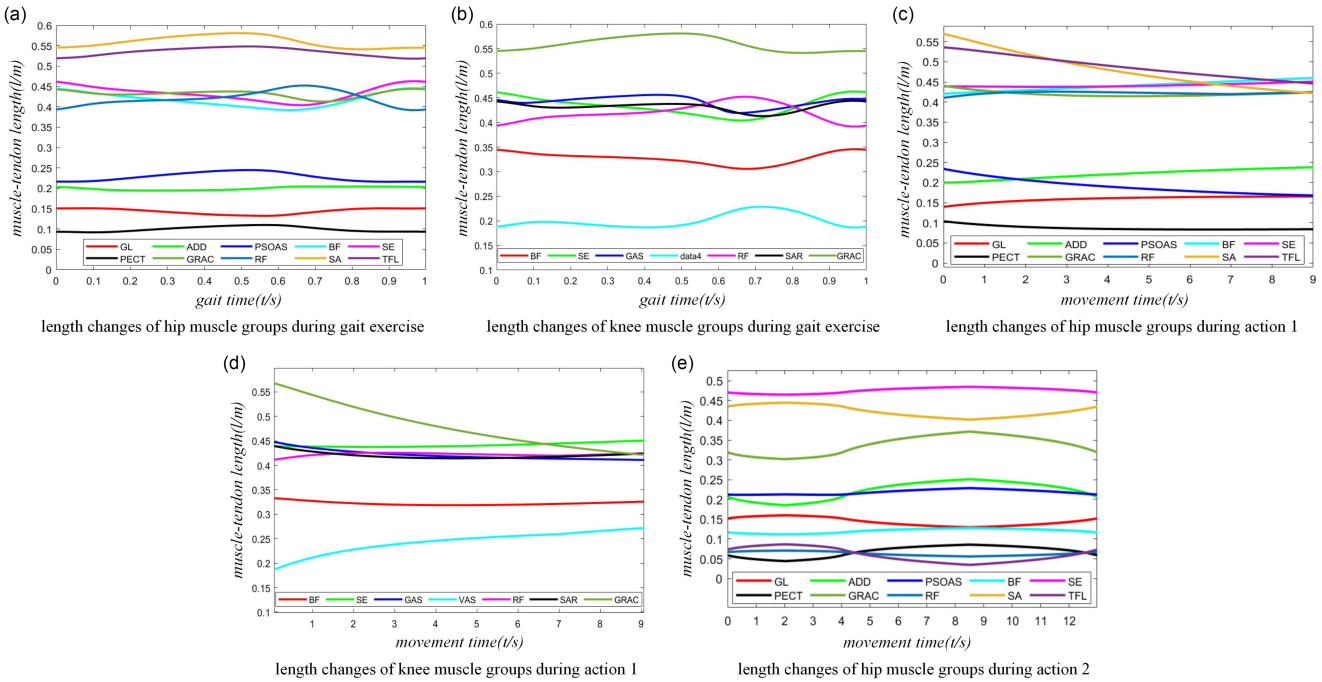

Table 4
Muscle activity of hip and knee-related muscle groups

Hip and knee-related motor muscle groups	Gait movement/m		Action 1/m		Action 2/m
	hip	knee	hip	knee	hip
GL	0.0186	/	0.0260		0.0306
ADD	0.0098	/	0.0384		0.0658
PSOAS	0.0286	/	0.0661		0.0169
BF	0.0536	0.0410	0.0397		0.0157
SE	0.0588	0.0588	0.0128		0.0198
GRAC	0.0312	0.0312	0.0260		0.0395
PECT	0.0182	/	0.0205		0.0216
RF	0.0604	0.0604	0.0154		0.0146
SA	0.0104	0.0104	0.0174		0.0427
TFL	0.0299	/	0.0897		0.0520
GAS	/	0.0369	0.0377		/
VAS	/	0.0420	0.0869		/

movement, while the muscle changes of the long head of the biceps femoris and the short head of the biceps femoris need to be considered together when analyzing the knee joint movement. The degree of muscle-tendon activity during contraction is the muscle activity m, which reflects the amount of muscle-tendon change from the shortest to the longest in a single exercise cycle, and the muscle activity of each muscle in the corresponding state is calculated from the above data on muscle-tendon length change. The values of muscle activity of the hip and knee muscle groups for the gait movement, movement 1, and movement 2 are shown in Table 4 and Figure 18.

During gait movements, the hip muscle groups BF, SE, and RF had the highest activity levels of 0.0536 m, 0.0538 m, and 0.0640 m, respectively, and they play a role in hip extension and knee flexion for the lower extremity. The activities of the other muscles in order of magnitude were GRAC, TFL, PSOAS, PECT, GL, SA, and ADD, which ranged from 0.0098 m to 0.0312 m. The adductor group ADD had the lowest activity of 0.0098 m. The adductor group is used to assist in maintaining balance of the trunk and lower extremities and requires less muscle activity. The knee muscle groups RF and SE had the greatest variation in activity at 0.0604 m and 0.0588 m. The activity of the other muscles in order of size was VAS, BF, GAS, GRAC, and SA, with length variations ranging from 0.0104 m to 0.0420 m. The sartorius muscle SA had the smallest activity of 0.0104 m, and it was involved in abduction and internal rotation of the hip joint, its length varied less during walking when the abduction and internal rotation movements of the hip joint were smaller in amplitude.

The range of motion of hip anterior flexion angle and knee posterior extension angle was significantly improved by 333% and 225%, respectively, for Action 1 compared to the muscle activity of human walking, during which the muscle activity of PSOAS, TFL, and VAS was significantly increased by 0.0661 m, 0.0897 m, and 0.0869 m, with the enhancement rates of 131%, 200%, and 107%, respectively, while GL, ADD, GRAC, PECT, SA, and GAS also showed an increase in muscle activity with lift rates in the range of 2.16% to 39.8%. However, the muscle activity of BF, SE, and RF was relatively reduced by 25.9%, 78.3%, and 16.7% to 0.0397 m, 0.0128 m, and 0.0154 m, respectively. The amplitude of hip adduction and abduction movements is small when the human body walks, and the hip adduction and abduction movements can be complemented by

Figure 18
Gait movement, action 1 and action 2 hip and knee joint-related muscle group muscle activity

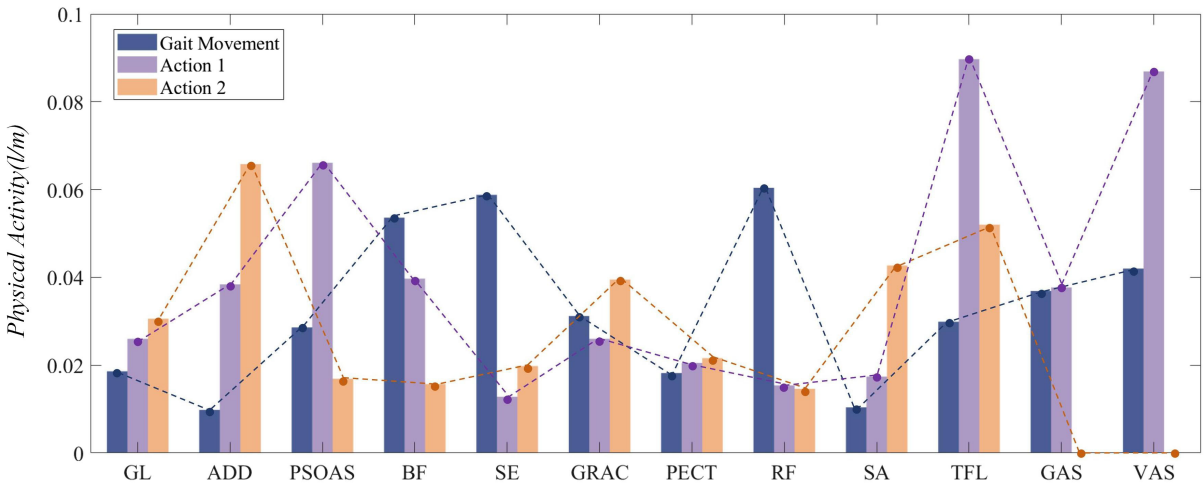

action 2. During movement 2, comparing the gait movement, the muscle activity of ADD and SA increased significantly with lengths of 0.0658 m and 0.0427 m and lift rates of 571% and 310%. In addition, GL, GRAC, PECT, and TFL also showed an increase in muscle activity with lift rates in the range of 64% to 73.9%. On the other hand, PSOAS, BF, SE, and RF showed a relative decrease in muscle activity with lengths of 0.0169 m, 0.0157 m, 0.0198 m, and 0.0146 m, which were 40.1%, 60.8%, 56.4%, and 75.9%, respectively.

For both rehabilitation exercises, Exercise 1 significantly enhanced the range of motion of hip anterior flexion and knee posterior extension, as well as the activity of the associated muscles. However, the activity of hip adduction and abduction-related muscles was relatively low, which was supplemented by exercise 2, which enhanced the adduction and abduction angle and the activity of related muscles. Comparing the activities of the hip and knee joints of the lower limbs under the integration of the two sets of exercises with those of the lower limbs under the walking condition, the activities of the hip and knee joints were significantly improved during the rehabilitation exercises, which can provide effective rehabilitation effects for the lower limbs.

5. Conclusion

This paper addresses the limitations of existing lower limb rehabilitation robots, which offer a limited range of rehabilitation movements and do not provide an intuitive analysis of their impact on human musculoskeletal issues. To overcome these limitations, a horizontal lower limb rehabilitation robot was designed to facilitate anterior flexion and posterior extension, as well as adduction and abduction movements of the hip joint, along with anterior flexion and posterior extension of the knee joint. A recumbent musculoskeletal model was developed by modifying the gait musculoskeletal model, and a coupling model was established to integrate the recumbent posture with the lower limb rehabilitation robot. OpenSim software was then used to simulate the motion of both the gait musculoskeletal model and the recumbent coupling model, analyzing changes in the length of the corresponding muscle-tendon units at the hip and knee joints. The simulation results indicate that rehabilitation training using the recumbent musculoskeletal model significantly enhances muscle activity in major muscle groups compared to gait motion. These findings demonstrate the effectiveness of the lower limb rehabilitation robot and provide theoretical support for its optimal design through human-machine coupling model simulations.

Although the designed rehabilitation robot can theoretically simulate the rehabilitation movements of the lower limbs of different patients, there are still some issues that need to be addressed. These include the need to address the wearing error between the robot and the patient, as well as analyzing the interaction force between the rehabilitation robot and the human body, which can better ensure the safety of the rehabilitation process.

In the future, detailed motion analysis will be performed on mannequins at different exercise speeds, focusing on comparing the effects of different exercise speeds on muscle activation. This study will help to find the optimal rehabilitation speed for more efficient rehabilitation. In addition, an in-depth analysis of the force changes of the lower limb muscles and the metabolic process of the muscles under the human-robot coupled movement state will follow. This will further validate the effectiveness of the rehabilitation robot and ensure its reliability and adaptability under different exercise conditions, thus providing more scientific and precise guidance for rehabilitation treatment.

Acknowledgement

The authors would like to thank all the anonymous reviewers for their helpful suggestions.

Funding Support

This work is sponsored by Jiangsu Basic Research Program (BK20210941), Changzhou Science and Technology Bureau (CE20225045).

Conflicts of Interest

The authors declare that they have no conflicts of interest to this work.

Data Availability Statement

Data sharing is not applicable to this article as no new data were created or analyzed in this study.

Author Contribution Statement

Yifan Zhao: Conceptualization, Methodology, Software, Formal analysis. **Quanyu Wu:** Resources, Data curation, Writing – original draft, Funding acquisition. **Jiaqi Fan:** Writing – review & editing, Visualization. **Shuyan Xiao:** Software, Supervision. **Yongxing Wang:** Project administration. **Xiaojie Liu:** Validation, Investigation. **Lingjiao Pan:** Methodology, Formal analysis.

References

[1] Guo, C., & Zheng, X. (2018). Health challenges and opportunities for an aging China. *American Journal of Public Health*, *108*(7), 890–892. https://doi.org/10.2105/AJPH.2018.304444

[2] Yao, Y. K., Zhang, Z. Q., Qi, M., Xu, J. S., Meng, Y., Li, H. H., …, & Zhang, G. Q. (2021). Quē xiě xìng nǎo cù zhōng huànzhě fābìng hòu bùtóng shíqí shēnghuó zhìliàng de yǐngxiǎng yīnsù yánjiū [Factors associated with quality of life in patients with ischemic stroke at different periods]. *Chinese General Practice*, *24*(33), 4200–4205. https://doi.org/10.12114/j.issn.1007-9572.2021.02.041

[3] Jin, P., Gao, F. X., Zhang, L., Tao, G. M., Huang, J., Kan, Z., & Jin, L. (2023). Kāngfù jīqìrén yánjiū dòngtài [Research trends in rehabilitation robots]. *Chinese Journal of Ergonomics*, *29*(1), 75–80. https://doi.org/10.13837/j.issn.1006-8309.2023.01.0014

[4] Wang, Y. Y. (2023). Xiàzhī wài gǔgé kāngfù jīqìrén yìngyòng yú nǎo cù zhōng piāntān xiàzhī yùndòng gōngnéng zhàng'ài huànzhě de xiàoguǒ [The effects of lower limb exoskeleton rehabilitation robots on motor function impairment in patients with hemiplegic lower limbs due to stroke]. *Chinese and Foreign Medical Research*, *21*(6), 132–135. https://doi.org/10.14033/j.cnki.cfmr.2023.06.033

[5] Cheng, X., Bai, D. Q., & Peng, X. H. (2021). Xiàzhī wài gǔgé kāngfù jīqìrén zài nǎo cù zhōng kāngfù zhōng de yìngyòng hé

yánjiū jìnzhǎn [Application and research progress of lower-limb exoskeleton rehabilitation robots in stroke rehabilitation]. *Chinese Journal of Rehabilitation Medicine*, *36*(10), 1327–1332. https://doi.org/10.3969/j.issn.1001-1242.2021.10.026

[6] Du, Y. C., Zhang, X., & Yu, H. L. (2022). Xiàzhī kāngfù jīqìrén yánjiū xiànzhuàng [Research status of lower limb rehabilitation robots]. *Progress in Biomedical Engineering*, *43*(2), 88–91. https://doi.org/10.3969/j.issn.1674-1242.2022.02.007

[7] Cao, H. Y., Tan, J. J., & Li, Y. (2022). Chuāndài shì xiàzhī zhù xíng qì [Wearable lower-limb assistive walker]. *Journal of Machine Design*, *39*(10), 165. https://doi.org/10.13841/j.cnki.jxsj.2022.10.012

[8] Plaza, A., Hernandez, M., Puyuelo, G., Garces, E., & Garcia, E. (2023). Wearable rehabilitation exoskeletons of the lower limb: Analysis of versatility and adaptability. *Disability and Rehabilitation: Assistive Technology*, *18*(4), 392–406. https://doi.org/10.1080/17483107.2020.1858976

[9] Li, H. Y., Feng, Y. F., Liu, G. W., Peng, X., Niu, J. Y., & Yin, D. Y. (2022). Zuò wò shì xiàzhī kāngfù jīqìrén de jīgòu shèjì yǔ fāngzhēn [Mechanism design and simulation of a sitting-lying lower limb rehabilitation robot]. *Machinery*, (7), 35–40. https://doi.org/10.3969/j.issn.1000-4998.2022.07.008

[10] Mu, H. F., Guo, K., & Hu, B. (2022). Jīyú móhú RBF shénjīng wǎngluò de kāngfù jīqìrén kòngzhì [Rehabilitation robot control based on fuzzy RBF neural network]. *Journal of Heilongjiang University of Technology (Comprehensive Edition)*, *22*(1), 75–79. https://doi.org/10.16792/j.cnki.1672-6758.2022.01.027

[11] Yan, B. B., Wu, H. H., Bi, R., Ma, C. Y., & Du, Y. M. (2023). Jīyú OpenSim de réntǐ xiàzhī shēngwù lìxué xìngnéng fāngzhēn shíyàn [Simulation experiment of human lower limb biomechanical performance based on OpenSim]. *Experimental Technology and Management*, *40*(8), 120–125. https://doi.org/10.16791/j.cnki.sjg.2023.08.018

[12] Song, J. K., Wei, J., Yu, B., Liu, C. L., Ai, C. J., & Zhang, J. J. (2023). Configuration design and kinematic performance analysis of a novel 4-DOF parallel ankle rehabilitation mechanism with two virtual motion centers. *Chinese Journal of Mechanical Engineering*, *36*(1), 154. https://doi.org/10.1186/s10033-023-00977-4

[13] Delgado, P., Alekhya, S., Majidirad, A., Hakansson, N. A., Desai, J., & Yihun, Y. (2020). Shoulder kinematics assessment towards exoskeleton development. *Applied Sciences*, *10*(18), 6336. https://doi.org/10.3390/app10186336

[14] Gordon, D. F., Christou, A., Stouraitis, T., Gienger, M., & Vijayakumar, S. (2023). Adaptive assistive robotics: A framework for triadic collaboration between humans and robots. *Royal Society Open Science*, *10*(6), 221617. https://doi.org/10.1098/rsos.221617

[15] Fan, Z. Z., Luo, R. M., Dai, R., & Sun, S. J. (2022). Jīyú OpenSim rén jī ǒuhé fāngzhēn de wài gǔgé shèjì fāngfǎ [Exoskeleton design method based on OpenSim human-machine coupling simulation]. *Journal of Machine Design*, *39*(3), 123–129. https://doi.org/10.13841/j.cnki.jxsj.2022.03.015

[16] Shi, C. Q., Han, Y. L., Chang, J. Z., Sun, H., Jin, Z. Z., & Zhu, W. L. (2022). Jīyú OpenSim de xiàzhī wài gǔgé jīqìrén fāngzhēn yánjiū [Simulation study of lower limb exoskeleton robot based on OpenSim]. *Journal of Nanjing Institute of Technology (Natural Science Edition)*, *20*(2), 45–49. https://doi.org/10.13960/j.issn.1672-2558.2022.02.008

[17] Feng, B. L., Song, P., Li, R. Y., Wei, Z. B., Li, Q., & Sun, X. C. (2024). Jīyú OpenSim de róuxìng xiàzhī zhùlì wài gǔgé shèjì jí fāngzhēn fēnxī [Design and simulation analysis of a flexible lower-limb assistive exoskeleton based on OpenSim]. *Journal of Mechanical Transmission*, *48*(5), 62–66. https://doi.org/10.16578/j.issn.1004.2539.2024.05.009

[18] Li, K. Q., Yao, G. L., Wu, Q. Y., Pan, L. J., & Liu, X. J. (2024). Réntǐ xiàzhī kāngfù yùndòng yìtú shìbié yǔ rén jī jiāohù xùnliàn fāngfǎ yánjiū [Research on recognition of human lower limb rehabilitation movement intention and human-machine interaction training methods]. *Journal of Chifeng University (Natural Science Edition)*, *40*(4), 11–15. https://doi.org/10.13398/j.cnki.issn1673-260x.2024.04.010

[19] Zhan, X. T., Chen, Q., & Li, Z. Y. (2019). Jīyú OpenSim de yāobù jī gǔ xìtǒng zài tǐ qián qū zhuàngtài xià shēngwù lìxué fēnxī [Biomechanical analysis of the lumbar musculoskeletal system in forward bending position based on OpenSim]. *Journal of Medical Biomechanics*, *34*(1), 27–34. https://doi.org/10.16156/j.1004-7220.2019.01.005

[20] Holmes, J. W. (2006). Teaching from classic papers: Hill's model of muscle contraction. *Advances in Physiology Education*, *30*(2), 67–72. https://doi.org/10.1152/advan.00072.2005

[21] Günther, M., & Schmitt, S. (2010). A macroscopic ansatz to deduce the Hill relation. *Journal of Theoretical Biology*, *263*(4), 407–418. https://doi.org/10.1016/j.jtbi.2009.12.027

[22] Dembia, C. L., Bianco, N. A., Falisse, A., Hicks, J. L., & Delp, S. L. (2020). OpenSim Moco: Musculoskeletal optimal control. *PLOS Computational Biology*, *16*(12), e1008493. https://doi.org/10.1371/journal.pcbi.1008493

[23] Thelen, D. G. (2003). Adjustment of muscle mechanics model parameters to simulate dynamic contractions in older adults. *Journal of Biomechanical Engineering*, *125*(1), 70–77. https://doi.org/10.1115/1.1531112

[24] Muller, A., Pontonnier, C., & Dumont, G. (2020). Motion-based prediction of hands and feet contact efforts during asymmetric handling tasks. *IEEE Transactions on Biomedical Engineering*, *67*(2), 344–352. https://doi.org/10.1109/TBME.2019.2913308

[25] Porsa, S., Lin, Y.-C., & Pandy, M. G. (2016). Direct methods for predicting movement biomechanics based upon optimal control theory with implementation in OpenSim. *Annals of Biomedical Engineering*, *44*(8), 2542–2557. https://doi.org/10.1007/s10439-015-1538-6

[26] Pan, F. Y., Jia, Y. B., Yang, M. H., Lü, Y. F., Zhao, J., Hao, Z. X., & Wang, R. C. (2023). Wò zī xiàzhī kāngfù xùnliàn yùndòng shēngwù lìxué tèxìng [Biomechanical characteristics of lower limb rehabilitation training in supine position]. *Journal of Tsinghua University (Science and Technology)*, *63*(12), 1984–1993. https://doi.org/10.16511/j.cnki.qhdxxb.2023.22.028

[27] Xu, H. H., He, Y. M., Sun, C. Y., & Guo, C. (2019). AnyBody huánjìng xià réntǐ bù tài de nìxiàng dònglì xué yánjiū [Inverse dynamics of human gait in AnyBody environment]. *Mechanical Science and Technology for Aerospace*

Engineering, *38*(12), 1819–1824. https://doi.org/10.13433/j.cnki.1003-8728.20190069

[28] Shuai, J. F., Wu, H. H., Yin, B. L., Ma, C. Y., & Yan, B. B. (2024). Píngdì xíngzǒu móshì xià jī gǔ cānshù duì jīròu dàixiè de yǐngxiǎng [Influence of musculoskeletal parameters on muscle metabolism under level walking mode]. *Mechanical Science and Technology for Aerospace Engineering*, *43*(2), 218–224. https://doi.org/10.13433/j.cnki.1003-8728.20220234

[29] Ma, X. Z., Niu, Y. G., Huo, H. F., & Zhao, H. (2024). OpenSim huánjìng xià qīngnián nánxìng qǐdòng bù tài de xiàzhī shēngwù lìxué tèzhēng yánjiū [Biomechanical characteristics of lower limbs in young male initiation gait under OpenSim environment]. *Mechanical Science and Technology for Aerospace Engineering*, *43*(9), 1551–1558. https://doi.org/10.13433/j.cnki.1003-8728.20230053

[30] Wang, C. J., Ma, J. W., & Cheng, B. (2024). Xī huái kāngfù fāngshēng jīqìrén de shèjì yǔ yùndòng fēnxī [Design and motion analysis of a knee-ankle rehabilitation bionic robot]. *Journal of Anhui University of Science and Technology (Natural Science)*, (5), 28–37. https://doi.org/10.3969/j.issn.1672-1098.2024.05.004

How to Cite: Zhao, Y., Wu, Q., Fan, J., Xiao, S., Wang, Y., Liu, X., & Pan, L. (2026). Design and Simulation Research of Supine Rehabilitation Robot. *Artificial Intelligence and Applications*, *4*(1), 111–124. https://doi.org/10.47852/bonviewAIA52024795